





# Collaborative Control for Aerial Transportation of Cargo With Dual Quadrotors

Zhuang Zhang, Hai Yu , *Student Member, IEEE*, Huiying Ye, Jianda Han , *Member, IEEE*,  
Yongchun Fang , *Senior Member, IEEE*, and Xiao Liang , *Senior Member, IEEE*

## I. INTRODUCTION

**Abstract**—With excellent maneuver performance and flexibility, quadrotor unmanned aerial vehicles (UAVs) are widely used in aerial transportation. However, the aerial transportation system with dual quadrotors exhibits high degrees of freedom, strong nonlinearities, and complex state couplings, which makes it more difficult to realize simultaneous quadrotor positioning and cargo swing suppression. Compared with the traditional description of cargo swing dynamics with four angles in the previous work, the spatial swing angle is introduced in a more intuitive way to reflect the swing dynamics of the cargo. On this basis, the dynamic model of the system is established according to Lagrange's equations. Then, a nonlinear adaptive controller is proposed, in which a dynamic compensation term is introduced to compensate for the lateral forces along the cables, and a spatial swing angle-related term is designed to enhance cargo swing damping. Meanwhile, considering the influence of unknown air resistance on quadrotors and cargo during transportation, an adaptive term is applied. Subsequently, Lyapunov techniques and LaSalle's invariance principle are used to prove the stability of the closed-loop system. Finally, based on the self-built general experimental platform, both indoor and outdoor experiments have been carried out to validate the practicability and effectiveness of the proposed method.

**Index Terms**—Aerial transportation systems, antising, collaborative control.

OWNING to the advantages of low cost, simple structure, and easy implementation, quadrotor unmanned aerial vehicles (UAVs) have been widely used in many fields and the control problem has become a research hotspot in the past decades [1], [2], [3], [4], [5], [6], [7], [8].

As a product of the progress of quadrotor applications, unmanned aerial transportation systems have received widespread attention from researchers. Some published works have adapted grippers [9], [10], [11], manipulators [12], [13], [14], and suspending cables [15], [16], [17], [18], [19], [20], [21], [22], [23], [24], [25], [26], [27], [28], [29], [30], [31], [32], [33], [34], [35] to complete transportation works. Usually, grippers and manipulators are mostly applied in cargo operation tasks, which are difficult to transport large cargoes due to the limited size of the end-effector. While the cable-suspended way is a low-cost transportation manner as it saves the development cost of the gripper and the manipulator. Therefore, from a practical application perspective, the cable-suspended way is widely used for aerial transportation, which can greatly preserve the maneuverability of quadrotors and the motion space of cargoes. For the aerial transportation system with a single quadrotor, some control methods have been proposed, such as input shaping [15], dynamic programming [16], [17],  $H_\infty$  [18], finite time control [19], adaptive control [20], [21], and methods based on neural network [22], [23].

However, when the cargo exceeds the carrying capacity of a single quadrotor, it is necessary to use multiple quadrotors for collaborative aerial transportation. Although the collaboration of multiple quadrotors can significantly improve the load capacity, the difficulty of precise control has also greatly increased due to complex dynamic coupling and nonlinearity. Facing this problem, many methods have been put forward to handle the complicated system dynamics. Some research works based on leader-follower framework have been carried out [24], [25], [26], [27]. The control objective of the leader quadrotor is to track its desired trajectory, while the follower quadrotor is required to adjust the constraint internal force of the system and the relative position between quadrotors. In [24], the leader quadrotor equipped with an April Tag completes cargo transportation with the follower guided by visually recognizing the leader. By introducing the input shapers, Chen and Shan, [25] reduced the residual oscillations of the follower quadrotor and the cargo. In [26], the follower quadrotor guarantees compliance with the external force applied by the leader onto the cargo via an admittance controller. By only employing onboard sensors, the linear quadratic regulator (LQR) controller and linear Kalman filter are utilized to realize leader-follower collaboration

Received 15 December 2023; revised 30 June 2024 and 11 August 2024; accepted 27 August 2024. Date of publication 3 October 2024; date of current version 7 January 2025. This work was supported in part by the National Natural Science Foundation of China under Grant 62273187 and Grant 623B2054, in part by the Natural Science Foundation of Tianjin under Grant 23JCQNJC01930, in part by the Key Technologies R & D Program of Tianjin under Grant 23YFZCSN00060, and in part by Haihe Lab of ITAI under Grant 22HHXCJC00003. Paper no. TII-23-5077. (Zhuang Zhang and Hai Yu are co-first authors.) (Corresponding author: Xiao Liang.)

The authors are with the Tianjin Key Laboratory of Intelligent Robotics, College of Artificial Intelligence, Institute of Robotics and Automatic Information System, Nankai University, Tianjin 300350, China, and also with the Engineering Research Center of Trusted Behavior Intelligence, Ministry of Education, Nankai University, Tianjin 300350, China (e-mail: zhangzhuang@mail.nankai.edu.cn; yuhai@mail.nankai.edu.cn; yehuiying@mail.nankai.edu.cn; hanjianda@nankai.edu.cn; fangyc@nankai.edu.cn; liangx@nankai.edu.cn).

This article has supplementary downloadable material available at <https://doi.org/10.1109/TII.2024.3459077>, provided by the authors.

Digital Object Identifier 10.1109/TII.2024.3459077

transportation [27]. Also, some works deal with quadrotors as single systems [28], [29], [30], and compensate for the influence of cargo by control algorithm. In [28], an adaptive dynamic compensator is designed to handle the dynamic effects caused by the tethered cargo over the quadrotors, as well as those caused by each quadrotor over the other. In [29], a layered dynamic control structure composed of a kinematic null-space based formation controller and a dynamic compensator with a neural sliding mode controller is presented. A cargo distribution control law is designed in [30] to equalize the load applied to the cables, and plenty of experimental tests are conducted by using two Yamaha RMAX helicopters. In addition, based on null-space theory, a kinematic formation controller [31] is designed for the dual helicopter transportation system to complete collision avoidance, wind disturbance resistance, and reasonable load distribution, and satisfactory results are obtained by introducing the spatial swing angle. Nevertheless, accurate system dynamic models with consideration of cargo motion are the basis of high-performance control, particularly, in cargo trajectory tracking or swing elimination. To improve control performance, some control schemes are designed based on the entire collaborative aerial transportation system model [32], [33], [34]. In [32], a nonlinear adaptive controller is constructed such that the cargo asymptotically follows a given desired trajectory for its position and attitude in the presence of uncertainties. In [33], an adaptive constrained formation control architecture is developed, in which universal barrier functions are constructed to address the time-varying relative position constraints, and adaptive estimators are employed to deal with system uncertainties. By constructing the generalized displacement signal of the cargo, a nonlinear adaptive control scheme is proposed in [34], which enhances the suppression effect of the cargo swing.

To sum up, compared with single quadrotor transportation system, due to the increase in the number of quadrotors, the collaborative aerial transportation systems present higher degrees of freedom, stronger nonlinearity, and more complex state coupling. Particularly, for the dual quadrotor transportation system, owing to its underactuated characteristics, the cargo swing can only be indirectly controlled through the control of the quadrotors. Therefore, achieving smooth cargo delivery using the dual quadrotor aerial transportation system is a highly challenging task. However, in most current research on dual quadrotor transportation systems [24], [26], [28], [29], [30], comprehensive modeling is not conducted, which means that the cargo dynamic is not fully considered in the system, making the suppression of cargo swing particularly difficult. To overcome the aforementioned difficulties, Chai et al. [34] constructed a quadrotor-cargo unified single to realize rapid cargo swing suppression, unfortunately, it only addresses the system in the transverse plane. Liang et al. [35] established a 3-D model for the dual quadrotor transportation system and achieved the cargo swing suppression by injecting damping based on the cargo swing angles' velocity. However, using four swing angles to represent the swing of a point cargo is not intuitive enough. In [31], the spatial swing angle is selected to analyze the cargo swing characteristics in 3-D space. Based on this, the dynamic model of the system is established by the Lagrange's equation. Subsequently, a nonlinear adaptive controller is designed on the basis of energy analysis, which can achieve accurate positioning of quadrotors, compensate for lateral forces along the cables, and suppress cargo swing under the circumstances of unknown air resistance coefficients. By rigorous analysis, the asymptotic

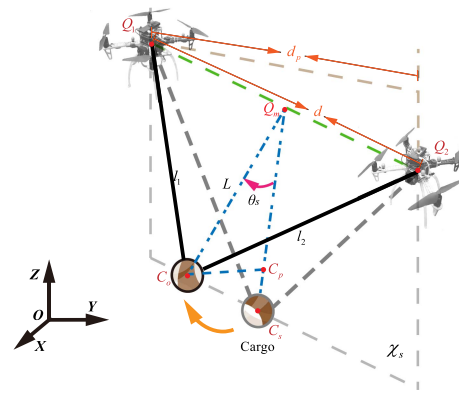


Fig. 1. Aerial collaborative transportation with dual quadrotors.

stability of the system can be proven. Finally, a self-built experimental platform applicable for both indoor and outdoor environments is designed, and the effectiveness of the proposed method is verified. Briefly speaking, the main contributions of this article can be summarized as follows.

- 1) Due to the stronger nonlinearity and complex state coupling, the cargo swing dynamics of the collaborative aerial transportation system are usually not fully considered [24], [26], [28], [29], [30]. Compared with the description of cargo swing dynamics with four angles in the previous work [35], the spatial swing angle can intuitively reflect the swing dynamics of the cargo. In addition, the spatial swing angle measurement device is devised and utilized to realize cooperative transportation.
- 2) Without model linearization or other simplification operations, a novel nonlinear adaptive controller is designed for the outer loop subsystem. Specifically, a dynamic compensation term is introduced to compensate for the lateral forces along the cables, and a spatial swing angle-related term is designed to enhance cargo swing damping. Meanwhile, considering the influence of unknown air resistance on quadrotors and cargo during transportation, an adaptive term is applied to the controller.
- 3) The constructed hardware platform avoids the dependence on external perception devices and only requires onboard sensors to achieve system state measurements, which has practical engineering significance. Based on the self-built general experimental platform, both indoor and outdoor validation experiments have been carried out.

The rest of this article is organized as follows. In Section II, the specific form of the spatial swing angle is defined and the dynamic equations of the system are provided. In Section III, the nonlinear adaptive controller development procedure and the design of update law for unknown air resistance parameters are illustrated in detail. Subsequently, the corresponding stability analysis is provided in Section IV. Section V presents the indoor and outdoor experimental results. Finally, Section VI concludes this article and the future work is summarized.

## II. PROBLEM FORMULATION

The aerial collaborative transportation system is depicted in Fig. 1, where the cargo is suspended by dual quadrotors via

cables.  $O_{xyz}$  is the inertial coordinate system,  $m_1$  and  $m_2$  represent the masses of the quadrotors,  $m_o$  is the mass of the cargo, and  $l_1$  and  $l_2$  are the lengths of the cables, respectively. The configurations of the two quadrotors are defined by the location of the center of mass  $\xi_1 = [x_1, y_1, z_1]^\top$ ,  $\xi_2 = [x_2, y_2, z_2]^\top$  and the attitude with respect to the inertial frame  $R_1, R_2 \in \text{SO}(3)$ .  $\xi_o = [x_o, y_o, z_o]^\top$  indicates the position of cargo in the swing process and  $\xi_s = [x_s, y_s, z_s]^\top$  denotes the position of cargo without cargo swing, corresponding to the stationary state.  $Q_1$  and  $Q_2$  denote the points of the center of mass of the quadrotors,  $C_o$  and  $C_s$  denote the points of the cargo in swing and without swing, respectively. Similar to many literatures for the cable-suspended aerial transportation systems [19], [20], [21], [27], [32], [33], [34], [35], [36], [37], [38], [39], the following reasonable assumption is made.

*Assumption 1:* The suspension cables connecting the cargo and the quadrotors are rigid.

### A. Dynamic Modeling

As provided in existing literature [35], the cargo swing is usually described by the angles of the suspension cables relative to the inertial coordinate system. For collaborative transportation with two quadrotors, four cable angles are required, which is overly redundant. In order to provide a more intuitive description of the cargo swing motion, we introduce the virtual suspension point  $Q_m$  and the virtual cable length  $L$ , and define the cargo swing angle as the spatial angle  $\theta_s$ . Specifically, the plane composed of the cargo and quadrotors is defined as  $\chi$ , in which the distance between quadrotors in the inertial frame is  $d = \|\xi_2 - \xi_1\|$  and represented by the green line in Fig. 1. The projected distance of quadrotors in the  $X$ - $Y$  plane is defined as  $d_p = \sqrt{(x_2 - x_1)^2 - (y_2 - y_1)^2}$ , which is represented by the brown dashed line. Then, draw the perpendicular to line  $Q_1Q_2$  through point  $C_o$ , and denote the intersection point as  $Q_m$ , whose coordinate is  $\xi_m = [x_m, y_m, z_m]^\top$ .  $Q_m$  is defined as the virtual suspending point, while line  $Q_mC_o$  is defined as the virtual cable, whose length is  $L$ . Define the plane  $\chi$  without the cargo swing as  $\chi_s$ . The angle between  $\chi$  and  $\chi_s$ , i.e.,  $\theta_s$ , is defined to describe the cargo swing.

The intersection of the planes  $\chi$  and  $\chi_s$  coincides with line  $Q_1Q_2$ . Thus, the angle between  $\chi$  and  $\chi_s$  can be described by the angle between the virtual cable and its projection on the plane  $\chi_s$ , i.e., line  $Q_mC_s$ , which is defined as the spatial swing angle  $\theta_s$ . The above defined state quantities are all related to the positions of quadrotors  $\xi_1, \xi_2$  and the spatial swing angle  $\theta_s$ .  $d_m$  is defined as the ratio of line  $Q_1Q_m$  to the line  $Q_1Q_2$ . The virtual suspending point  $Q_m$  is calculated by the geometric relationship according to the relative position between the quadrotors and the cables, which is presented as follows:

$$d_m = \frac{l_1^2 - l_2^2 + d^2}{2d^2}, L = \sqrt{l_1^2 - (d_m d)^2}$$

$$x_m = x_1 + d_m \Delta x, y_m = y_1 + d_m \Delta y, z_m = z_1 + d_m \Delta z$$

where  $\Delta x = x_2 - x_1, \Delta y = y_2 - y_1, \Delta z = z_2 - z_1$ . By projecting  $C_o$  to  $X$ - $Y$  plane and  $\chi$  plane, respectively, the position of cargo can be presented as follows:

$$x_o = x_m + \frac{\Delta y \Delta z L \cos \theta_s}{dd_p} + \frac{\Delta y}{d_p} L \sin \theta_s \quad (1)$$

$$y_o = y_m + \frac{\Delta y \Delta z L \cos \theta_s}{dd_p} + \frac{\Delta x}{d_p} L \sin \theta_s \quad (2)$$

$$z_o = z_m - \frac{d_p L \cos \theta_s}{d} \quad (3)$$

Based on (1)–(3), the kinetic energy and the potential energy of the quadrotors and the cargo can be obtained as follows:

$$T = \frac{1}{2} m_1 \dot{\xi}_1^\top \dot{\xi}_1 + \frac{1}{2} m_2 \dot{\xi}_2^\top \dot{\xi}_2 + \frac{1}{2} m_o \dot{\xi}_o^\top \dot{\xi}_o \quad (4)$$

$$H = m_1 g z_1 + m_2 g z_2 + m_o g z_o \quad (5)$$

By choosing the generalized coordinate vector as  $\mathbf{q} = [\xi_1^\top, \xi_2^\top, \theta_s]^\top = [x_1, y_1, z_1, x_2, y_2, z_2, \theta_s]^\top$ , the Lagrange function can be expressed in the following form:

$$\frac{d}{dt} \frac{\partial L}{\partial \dot{\mathbf{q}}} - \frac{\partial L}{\partial \mathbf{q}} = \mathbf{F}_T \quad (6)$$

where  $L = T - H$  is the Lagrangian. The external forces on the system include the thrusts generated by the motors, as well as the resistance  $\mathbf{f}_{q1}, \mathbf{f}_{q2}, \mathbf{f}_c$  acting on the quadrotors and the cargo. The resistance can be expressed as follows:

$$\mathbf{f}_{q1} = -D_{q1} \dot{\xi}_1, \mathbf{f}_{q2} = -D_{q2} \dot{\xi}_2, \mathbf{f}_c = -D_c \dot{\xi}_o$$

where  $D_{q1} = \text{diag}([d_{1x}, d_{1y}, d_{1z}])$ ,  $D_{q2} = \text{diag}([d_{2x}, d_{2y}, d_{2z}])$ , and  $D_c = \text{diag}([d_{cx}, d_{cy}, d_{cz}]) \in \mathbb{R}_+^{3 \times 3}$  represent the resistance coefficient matrices of quadrotors and cargo. The virtual work  $\delta W$  along the virtual displacement of quadrotors and cargo  $\delta \xi_1, \delta \xi_2$ , and  $\delta \xi_o$  is as follows:

$$\delta W = (f_1 R_1 e_3 + \mathbf{f}_{q1})^\top \delta \xi_1 + (f_2 R_2 e_3 + \mathbf{f}_{q2})^\top \delta \xi_2 + \mathbf{f}_c^\top \delta \xi_o$$

where  $f_1, f_2 \in \mathbb{R}$  are the applied thrusts generated by quadrotors,  $e_3 = [0, 0, 1]^\top$ . In order to facilitate the expression of the generalized force on the cargo, the Jacobian matrix  $P_o \in \mathbb{R}^{3 \times 7}$  between the virtual displacement of cargo and the generalized coordinate  $\mathbf{q}$  is defined as follows:

$$\delta \xi_o = P_o \delta \mathbf{q} \quad (7)$$

where  $\rho_j = [\rho_{jx}, \rho_{jy}, \rho_{jz}]^\top \in \mathbb{R}^3, j = \{1, 2, \dots, 7\}$  is defined as the  $j$ th column vector of  $P_o$ . According to selected generalized coordinates, the generalized force can be calculated by  $F_{Tj} = \frac{\delta W}{\delta q_j}, j = \{1, 2, \dots, 7\}$ , which is further presented as follows:

$$\begin{aligned} F_{T1} &= f_1 R_{1(1,3)} - d_{1x} \dot{x}_1 + \mathbf{f}_c^\top \rho_1, \\ F_{T2} &= f_1 R_{1(2,3)} - d_{1y} \dot{y}_1 + \mathbf{f}_c^\top \rho_2, \\ F_{T3} &= f_1 R_{1(3,3)} - d_{1z} \dot{z}_1 + \mathbf{f}_c^\top \rho_3, \\ F_{T4} &= f_2 R_{2(1,3)} - d_{2x} \dot{x}_2 + \mathbf{f}_c^\top \rho_4, \\ F_{T5} &= f_2 R_{2(2,3)} - d_{2y} \dot{y}_2 + \mathbf{f}_c^\top \rho_5, \\ F_{T6} &= f_2 R_{2(3,3)} - d_{2z} \dot{z}_2 + \mathbf{f}_c^\top \rho_6, F_{T7} = \mathbf{f}_c^\top \rho_7 \end{aligned} \quad (8)$$

where  $f_1 R_1 e_3 = [f_1 R_{1(1,3)}, f_1 R_{1(2,3)}, f_1 R_{1(3,3)}]^\top$  and  $f_2 R_2 e_3 = [f_2 R_{2(1,3)}, f_2 R_{2(2,3)}, f_2 R_{2(3,3)}]^\top \in \mathbb{R}^3$ . Define the actuated control input vector  $\mathbf{u}_f = [(f_1 R_1 e_3)^\top, (f_2 R_2 e_3)^\top]^\top \in \mathbb{R}^6$ .

Subsequently, substituting (4) and (5) into (6), according to (8), the dynamic equations of the outer loop subsystem can be derived as follows:

$$M_c(\mathbf{q}) \ddot{\mathbf{q}} + V_c(\mathbf{q}, \dot{\mathbf{q}}) \dot{\mathbf{q}} + \mathbf{G}(\mathbf{q}) = \mathbf{F} + \mathbf{F}_a \quad (9)$$



where  $M_c(\mathbf{q}), V_c(\mathbf{q}, \dot{\mathbf{q}}) \in \mathbb{R}^{7 \times 7}$  and  $\mathbf{G}(\mathbf{q}), \mathbf{F} = [\mathbf{u}_f^\top, 0]^\top = [(f_1 R_1 \mathbf{e}_3)^\top, (f_2 R_2 \mathbf{e}_3)^\top, 0]^\top \in \mathbb{R}^7$  denote the inertia matrix, the centripetal-Coriolis matrix, the gravity vector, and the control inputs applied to the system, respectively.  $\mathbf{F}_a \in \mathbb{R}^7$  presents the resistance to the system. The entries of  $\mathbf{G}(\mathbf{q})$  are presented as follows:

$$G_1 = m_{og} \left[ \frac{\Delta x \Delta z (2d_m - 1)}{d^2} - \frac{\Delta x \cos \theta_s d_p L}{d^3} + \frac{\Delta x \cos \theta_s L}{d_p d} + \frac{2\Delta x \cos \theta_s d_p d_m (d_m - 1)}{2dL} \right] \quad (10)$$

$$G_2 = m_{og} \left[ \frac{\Delta y \Delta z (2d_m - 1)}{d^2} - \frac{\Delta y \cos \theta_s d_p L}{d^3} + \frac{\Delta y \cos \theta_s L}{d_p d} + \frac{2\Delta y \cos \theta_s d_p d_m (d_m - 1)}{2dL} \right] \quad (11)$$

$$G_3 = m_1 g + m_{og} \left[ 1 - \frac{\Delta z^2 (1 - 2d_m)}{d^2} - d_m - \frac{\Delta z \cos \theta_s d_p L}{d^3} + \frac{2\Delta z \cos \theta_s d_p d_m (d_m - 1)}{2dL} \right] \quad (12)$$

$$G_4 = m_{og} \left[ \frac{\Delta x \Delta z (1 - 2d_m)}{d^2} + \frac{\Delta x \cos \theta_s d_p L}{d^3} - \frac{\Delta x \cos \theta_s L}{d_p d} - \frac{2\Delta x \cos \theta_s d_p d_m (d_m - 1)}{2dL} \right], \quad (13)$$

$$G_5 = m_{og} \left[ \frac{\Delta y \Delta z (1 - 2d_m)}{d^2} + \frac{\Delta y \cos \theta_s d_p L}{d^3} - \frac{\Delta y \cos \theta_s L}{d_p d} - \frac{2\Delta y \cos \theta_s d_p d_m (d_m - 1)}{2dL} \right] \quad (14)$$

$$G_6 = m_2 g + m_{og} \left[ \frac{\Delta z^2 (1 - 2d_m)}{d^2} + d_m + \frac{\Delta z \cos \theta_s d_p L}{d^3} - \frac{2\Delta z \cos \theta_s d_p d_m (d_m - 1)}{2dL} \right] \quad (15)$$

$$G_7 = \frac{m_{og} d_p L \sin \theta_s}{d}. \quad (16)$$

According to (6), (10)–(16),  $\mathbf{G}$  can be divided into two following parts:

$$\begin{aligned} \mathbf{G} &= -\frac{\partial L}{\partial \mathbf{q}} = \frac{\partial H}{\partial \mathbf{q}} = \frac{\partial (m_1 g z_1 + m_2 g z_2)}{\partial \mathbf{q}} + \frac{\partial m_{og} z_o}{\partial \mathbf{q}} \\ &= \frac{\partial (m_1 g z_1 + m_2 g z_2 + m_{og} z_m)}{\partial \mathbf{q}} + \frac{\partial \frac{-m_{og} d_p L \cos \theta_s}{d}}{\partial \mathbf{q}} \\ &= \mathbf{G}_r + \mathbf{G}_s \end{aligned} \quad (17)$$

where  $\mathbf{G}_s$  is related to the spatial swing angle  $\theta_s$ . Define  $\mathbf{G}_o = [G_{o1}, G_{o2}, G_{o3}, G_{o4}, G_{o5}, G_{o6}, G_{o7}]^\top$  to be the special form of  $\mathbf{G}_s$  where  $\theta_s$  is zero. Similar to many other Lagrange systems [12], [13], [21], [34], [35], one can verify that model (9) satisfies the following property:

**Property 1:**  $M_c$  and  $V_c$  satisfy the skew-symmetric relationship, i.e.,  $\boldsymbol{\alpha}^\top (\frac{1}{2} \dot{M}_c - V_c) \boldsymbol{\alpha} = 0 \forall \boldsymbol{\alpha} \in \mathbb{R}^7$ .

## B. Control Objective

The control objective is to drive the quadrotors to move from their initial positions to the desired positions  $\boldsymbol{\xi}_{id} = [x_{id}, y_{id}, z_{id}]^\top$ ,  $i = 1, 2$ , and to guarantee that the spatial swing angle is suppressed during the flight process, which can be mathematically described as follows:

$$\boldsymbol{\xi}_1 \rightarrow \boldsymbol{\xi}_{1d}, \boldsymbol{\xi}_2 \rightarrow \boldsymbol{\xi}_{2d}, \theta_s \rightarrow 0.$$

The position errors of the two quadrotors are defined as  $\mathbf{e}_{\xi 1} = \boldsymbol{\xi}_1^\top - \boldsymbol{\xi}_{1d}^\top$  and  $\mathbf{e}_{\xi 2} = \boldsymbol{\xi}_2^\top - \boldsymbol{\xi}_{2d}^\top$ . Since the time derivative of the target positions are zeros, the time derivative of the quadrotors' position errors are  $\dot{\mathbf{e}}_{\xi 1} = \dot{\boldsymbol{\xi}}_1^\top$  and  $\dot{\mathbf{e}}_{\xi 2} = \dot{\boldsymbol{\xi}}_2^\top$ . For the convenience of subsequent controller development and analysis, combine the two quadrotors' position as vector  $\boldsymbol{\xi} = [\boldsymbol{\xi}_1^\top, \boldsymbol{\xi}_2^\top]^\top \in \mathbb{R}^6$ , and its desired value as  $\boldsymbol{\xi}_d = [\boldsymbol{\xi}_{1d}^\top, \boldsymbol{\xi}_{2d}^\top]^\top \in \mathbb{R}^6$ . Thus, combined position error is  $\mathbf{e}_\xi = \boldsymbol{\xi} - \boldsymbol{\xi}_d = [\mathbf{e}_{\xi 1}^\top, \mathbf{e}_{\xi 2}^\top]^\top$ , and its time derivative is  $\dot{\mathbf{e}}_\xi = \dot{\boldsymbol{\xi}}$ .

## III. CONTROLLER DEVELOPMENT

The energy function of the outer loop subsystem is given as follows:

$$E = \frac{1}{2} \dot{\mathbf{q}}^\top M_c \dot{\mathbf{q}} + \lambda = \frac{1}{2} \dot{\mathbf{q}}^\top M_c \dot{\mathbf{q}} + \frac{m_{og} d_p L}{d} (1 - \cos \theta_s) \quad (18)$$

where  $\lambda = \frac{m_{og} d_p L}{d} (1 - \cos \theta_s)$  is part of the potential energy difference between the swing state and the nonswing state of the cargo. According to (17), the derivative of  $\lambda$  with respect to time is as follows:

$$\begin{aligned} \dot{\lambda} &= \frac{d\lambda}{dt} = \frac{\partial \lambda}{\partial \mathbf{q}} \cdot \frac{d\mathbf{q}}{dt} = \dot{\mathbf{q}}^\top \frac{\partial \lambda}{\partial \mathbf{q}} = \dot{\mathbf{q}}^\top \left( \frac{\partial \frac{m_{og} d_p L}{d} (1 - \cos \theta_s)}{\partial \mathbf{q}} \right) \\ &= \dot{\mathbf{q}}^\top \left( \frac{\partial \frac{-m_{og} d_p L \cos \theta_s}{d}}{\partial \mathbf{q}} - \frac{\partial \frac{-m_{og} d_p L}{d}}{\partial \mathbf{q}} \right) \\ &= \dot{\mathbf{q}}^\top (\mathbf{G}_s - \mathbf{G}_o). \end{aligned} \quad (19)$$

Based on (9), (19), and Property 1, the time derivative of  $E(t)$  can be calculated as follows:

$$\begin{aligned} \dot{E} &= \dot{\mathbf{q}}^\top \left( \mathbf{F} + \mathbf{F}_a - \mathbf{G} - V_c \dot{\mathbf{q}} + \frac{1}{2} \dot{M}_c \dot{\mathbf{q}} \right) + \dot{\lambda} \\ &= \dot{\mathbf{q}}^\top \mathbf{F} + \dot{\mathbf{q}}^\top \mathbf{F}_a - \dot{\mathbf{q}}^\top (\mathbf{G}_r + \mathbf{G}_s) + \dot{\mathbf{q}}^\top (\mathbf{G}_s - \mathbf{G}_o) \\ &= \dot{\mathbf{q}}^\top [\mathbf{F} - (\mathbf{G}_r + \mathbf{G}_o)] + \dot{\mathbf{q}}^\top \mathbf{F}_a \end{aligned} \quad (20)$$

where  $\mathbf{G}_r + \mathbf{G}_o$  represents the tensions of the cables due to the gravity of the cargo, and varies with the motion of the quadrotors. From (10)–(17), one knows that the last element of  $\mathbf{G}_r + \mathbf{G}_o$  is zero. Thus, define  $\mathbf{G}_r + \mathbf{G}_o = [\mathbf{G}_t^\top, 0]^\top \in \mathbb{R}^7$ , where  $\mathbf{G}_t \in \mathbb{R}^6$  is the vector of the first six elements of  $\mathbf{G}_r + \mathbf{G}_o$ . The vector of the first six elements of  $\mathbf{F}_a$  is denoted as  $\mathbf{F}_\xi$ , while the seventh element is denoted as  $F_s = \mathbf{f}_c^\top \boldsymbol{\rho}_7$ . For the convenience of the subsequent derivation, based on (7), the velocity of cargo can be presented by  $\dot{\theta}_s$  as:  $\dot{\boldsymbol{\xi}}_o = \boldsymbol{\rho}_7 \dot{\theta}_s + \boldsymbol{\eta}$ . It is worth noting that  $\boldsymbol{\eta}$  contains velocity quantities of quadrotors, and the specific decomposition form will be presented later. Subsequently, (20) can be rewritten as follows:

$$\dot{E} = [\dot{\boldsymbol{\xi}}^\top, \dot{\theta}_s] \cdot ([\mathbf{u}_f^\top, 0]^\top - [\mathbf{G}_t^\top, 0]^\top) + [\dot{\boldsymbol{\xi}}^\top, \dot{\theta}_s] \cdot [\mathbf{F}_\xi^\top, F_s]^\top$$

$$= \dot{\xi}^\top (\mathbf{u}_f - \mathbf{G}_t) + \dot{\xi}^\top \mathbf{F}_\xi - \dot{\theta}_s (D_c \boldsymbol{\eta})^\top \boldsymbol{\rho}_7 - \dot{\theta}_s^2 \boldsymbol{\rho}_7^\top D_c \boldsymbol{\rho}_7. \quad (21)$$

To separate  $\dot{\xi}$  from  $\boldsymbol{\eta}$ , a mapping matrix  $Q \in \mathbb{R}^{3 \times 6}$  is introduced as follows:

$$\boldsymbol{\eta} = Q \dot{\xi}. \quad (22)$$

Then, to facilitate subsequent derivation,  $\boldsymbol{\mu}_i, i = 1, 2, \dots, 6$ , is defined as the  $i$ th column vector of  $Q$ , and  $\boldsymbol{\mu}_i = [\mu_{ix}, \mu_{iy}, \mu_{iz}]^\top$ . Substituting (22) into (21), one can obtain the following:

$$\begin{aligned} \dot{E} &= \dot{\xi}^\top (\mathbf{u}_f - \mathbf{G}_t) + \dot{\xi}^\top (\mathbf{F}_\xi - Q^\top D_c \boldsymbol{\rho}_7 \dot{\theta}_s) - \dot{\theta}_s^2 \boldsymbol{\rho}_7^\top D_c \boldsymbol{\rho}_7 \\ &= \dot{\xi}^\top (\mathbf{u}_f - \mathbf{G}_t - \boldsymbol{\Phi}) - \dot{\theta}_s^2 \boldsymbol{\rho}_7^\top D_c \boldsymbol{\rho}_7 \end{aligned} \quad (23)$$

where  $\boldsymbol{\Phi} = -\mathbf{F}_\xi + Q^\top D_c \boldsymbol{\rho}_7 \dot{\theta}_s$ , which can be linearly parameterized as follows:

$$\boldsymbol{\Phi} = [\phi_{x1}^\top \boldsymbol{\omega}_{x1}, \phi_{y1}^\top \boldsymbol{\omega}_{y1}, \phi_{z1}^\top \boldsymbol{\omega}_{z1}, \phi_{x2}^\top \boldsymbol{\omega}_{x2}, \phi_{y2}^\top \boldsymbol{\omega}_{y2}, \phi_{z2}^\top \boldsymbol{\omega}_{z2}]^\top. \quad (24)$$

Without loss of generality, the resistance coefficients for the cargo in all directions of motion are the same, i.e.,  $d_{cx} = d_{cy} = d_{cz} = d_c$ . Therefore, the details of the elements in (24) can be presented as follows:

$$\phi_{x1} = [\dot{x}_1, \dot{\xi}_o^\top \boldsymbol{\rho}_1 + \dot{\theta}_s \boldsymbol{\mu}_1^\top \boldsymbol{\rho}_7]^\top, \boldsymbol{\omega}_{x1} = [d_{x1}, d_c]^\top, \quad (25)$$

$$\phi_{y1} = [\dot{y}_1, \dot{\xi}_o^\top \boldsymbol{\rho}_2 + \dot{\theta}_s \boldsymbol{\mu}_2^\top \boldsymbol{\rho}_7]^\top, \boldsymbol{\omega}_{y1} = [d_{y1}, d_c]^\top, \quad (26)$$

$$\phi_{z1} = [\dot{z}_1, \dot{\xi}_o^\top \boldsymbol{\rho}_3 + \dot{\theta}_s \boldsymbol{\mu}_3^\top \boldsymbol{\rho}_7]^\top, \boldsymbol{\omega}_{z1} = [d_{z1}, d_c]^\top, \quad (27)$$

$$\phi_{x2} = [\dot{x}_2, \dot{\xi}_o^\top \boldsymbol{\rho}_4 + \dot{\theta}_s \boldsymbol{\mu}_4^\top \boldsymbol{\rho}_7]^\top, \boldsymbol{\omega}_{x2} = [d_{x2}, d_c]^\top, \quad (28)$$

$$\phi_{y2} = [\dot{y}_2, \dot{\xi}_o^\top \boldsymbol{\rho}_5 + \dot{\theta}_s \boldsymbol{\mu}_5^\top \boldsymbol{\rho}_7]^\top, \boldsymbol{\omega}_{y2} = [d_{y2}, d_c]^\top, \quad (29)$$

$$\phi_{z2} = [\dot{z}_2, \dot{\xi}_o^\top \boldsymbol{\rho}_6 + \dot{\theta}_s \boldsymbol{\mu}_6^\top \boldsymbol{\rho}_7]^\top, \boldsymbol{\omega}_{z2} = [d_{z2}, d_c]^\top. \quad (30)$$

According to (18) and (25)–(30), the new energy function can be constructed as follows:

$$\begin{aligned} V &= E + \frac{1}{2} e_\xi^\top K_p e_\xi + \frac{1}{2} \tilde{\boldsymbol{\omega}}_{x1}^\top \Gamma_{x1}^{-1} \tilde{\boldsymbol{\omega}}_{x1} + \frac{1}{2} \tilde{\boldsymbol{\omega}}_{y1}^\top \Gamma_{y1}^{-1} \tilde{\boldsymbol{\omega}}_{y1} \\ &\quad + \frac{1}{2} \tilde{\boldsymbol{\omega}}_{z1}^\top \Gamma_{z1}^{-1} \tilde{\boldsymbol{\omega}}_{z1} + \frac{1}{2} \tilde{\boldsymbol{\omega}}_{x2}^\top \Gamma_{x2}^{-1} \tilde{\boldsymbol{\omega}}_{x2} + \frac{1}{2} \tilde{\boldsymbol{\omega}}_{y2}^\top \Gamma_{y2}^{-1} \tilde{\boldsymbol{\omega}}_{y2} \\ &\quad + \frac{1}{2} \tilde{\boldsymbol{\omega}}_{z2}^\top \Gamma_{z2}^{-1} \tilde{\boldsymbol{\omega}}_{z2} \end{aligned} \quad (31)$$

where  $K_p = \text{diag}([k_{px1}, k_{py1}, k_{pz1}, k_{px2}, k_{py2}, k_{pz2}]) \in \mathbb{R}_+^{6 \times 6}$  is the positive control gain matrix, and  $\Gamma_{x1}, \Gamma_{y1}, \Gamma_{z1}, \Gamma_{x2}, \Gamma_{y2}, \Gamma_{z2} \in \mathbb{R}_+^{2 \times 2}$  are positive definite update gain matrices.  $\tilde{\boldsymbol{\omega}}_{x1}, \tilde{\boldsymbol{\omega}}_{y1}, \tilde{\boldsymbol{\omega}}_{z1}, \tilde{\boldsymbol{\omega}}_{x2}, \tilde{\boldsymbol{\omega}}_{y2}, \tilde{\boldsymbol{\omega}}_{z2}$  denote the estimation error whose detailed forms are as follows:

$$\begin{aligned} \tilde{\boldsymbol{\omega}}_{x1} &= \boldsymbol{\omega}_{x1} - \hat{\boldsymbol{\omega}}_{x1}, \tilde{\boldsymbol{\omega}}_{y1} = \boldsymbol{\omega}_{y1} - \hat{\boldsymbol{\omega}}_{y1}, \tilde{\boldsymbol{\omega}}_{z1} = \boldsymbol{\omega}_{z1} - \hat{\boldsymbol{\omega}}_{z1}, \\ \tilde{\boldsymbol{\omega}}_{x2} &= \boldsymbol{\omega}_{x2} - \hat{\boldsymbol{\omega}}_{x2}, \tilde{\boldsymbol{\omega}}_{y2} = \boldsymbol{\omega}_{y2} - \hat{\boldsymbol{\omega}}_{y2}, \tilde{\boldsymbol{\omega}}_{z2} = \boldsymbol{\omega}_{z2} - \hat{\boldsymbol{\omega}}_{z2}, \end{aligned} \quad (32)$$

where  $\hat{\boldsymbol{\omega}}_{x1}, \hat{\boldsymbol{\omega}}_{y1}, \hat{\boldsymbol{\omega}}_{z1}, \hat{\boldsymbol{\omega}}_{x2}, \hat{\boldsymbol{\omega}}_{y2}$ , and  $\hat{\boldsymbol{\omega}}_{z2}$  represent the estimate values of the resistance coefficients. The update law is designed in the following form:

$$\dot{\hat{\boldsymbol{\omega}}}_{x1} = -\Gamma_{x1} \phi_{x1} \dot{e}_{x1}, \dot{\hat{\boldsymbol{\omega}}}_{y1} = -\Gamma_{y1} \phi_{y1} \dot{e}_{y1},$$

$$\dot{\hat{\boldsymbol{\omega}}}_{z1} = -\Gamma_{z1} \phi_{z1} \dot{e}_{z1}, \dot{\hat{\boldsymbol{\omega}}}_{x2} = -\Gamma_{x2} \phi_{x2} \dot{e}_{x2},$$

$$\dot{\hat{\boldsymbol{\omega}}}_{y2} = -\Gamma_{y2} \phi_{y2} \dot{e}_{y2}, \dot{\hat{\boldsymbol{\omega}}}_{z2} = -\Gamma_{z2} \phi_{z2} \dot{e}_{z2}. \quad (33)$$

According to (20), (32), and (33), the time derivative of (31) can be calculated as follows:

$$\begin{aligned} \dot{V} &= \dot{e}_\xi^\top (\mathbf{u}_f - \mathbf{G}_t + K_p e_\xi) - \dot{\theta}_s^2 \boldsymbol{\rho}_7^\top D_c \boldsymbol{\rho}_7 - \dot{e}_{x1} \phi_{x1}^\top \hat{\boldsymbol{\omega}}_{x1} \\ &\quad - \dot{e}_{y1} \phi_{y1}^\top \hat{\boldsymbol{\omega}}_{y1} - \dot{e}_{z1} \phi_{z1}^\top \hat{\boldsymbol{\omega}}_{z1} - \dot{e}_{x2} \phi_{x2}^\top \hat{\boldsymbol{\omega}}_{x2} - \dot{e}_{y2} \phi_{y2}^\top \hat{\boldsymbol{\omega}}_{y2} \\ &\quad - \dot{e}_{z2} \phi_{z2}^\top \hat{\boldsymbol{\omega}}_{z2} \\ &= \dot{e}_\xi^\top (\mathbf{u}_f - \mathbf{G}_t + K_p e_\xi - \hat{\boldsymbol{\Phi}}) - \dot{\theta}_s^2 \boldsymbol{\rho}_7^\top D_c \boldsymbol{\rho}_7 \end{aligned} \quad (34)$$

where  $\hat{\boldsymbol{\Phi}} = [\phi_{x1}^\top \hat{\boldsymbol{\omega}}_{x1}, \phi_{y1}^\top \hat{\boldsymbol{\omega}}_{y1}, \phi_{z1}^\top \hat{\boldsymbol{\omega}}_{z1}, \phi_{x2}^\top \hat{\boldsymbol{\omega}}_{x2}, \phi_{y2}^\top \hat{\boldsymbol{\omega}}_{y2}, \phi_{z2}^\top \hat{\boldsymbol{\omega}}_{z2}]^\top$  denotes the estimated value vector. Based on the framework of hierarchical control [40], [41], [42],  $\mathbf{u}_f = [(f_1 R_1 \mathbf{e}_3)^\top, (f_2 R_2 \mathbf{e}_3)^\top]^\top$  can be divided into two parts, i.e.,  $\mathbf{u}_f = \mathbf{u} + \mathbf{u}_\Delta$  and  $\mathbf{u} = [\frac{f_1 (R_{1d} \mathbf{e}_3)^\top}{\mathbf{e}_3^\top R_{1d}^\top R_1 \mathbf{e}_3}, \frac{f_2 (R_{2d} \mathbf{e}_3)^\top}{\mathbf{e}_3^\top R_{2d}^\top R_2 \mathbf{e}_3}]^\top$  as follows:

$$\mathbf{u}_\Delta = \left[ \frac{f_1 ((\mathbf{e}_3^\top R_{1d}^\top R_1 \mathbf{e}_3) R_1 \mathbf{e}_3 - R_{1d} \mathbf{e}_3)^\top}{\mathbf{e}_3^\top R_{1d}^\top R_1 \mathbf{e}_3}, \frac{f_2 ((\mathbf{e}_3^\top R_{2d}^\top R_2 \mathbf{e}_3) R_2 \mathbf{e}_3 - R_{2d} \mathbf{e}_3)^\top}{\mathbf{e}_3^\top R_{2d}^\top R_2 \mathbf{e}_3} \right]^\top$$

where  $\mathbf{u}$  is the to-be-constructed virtual control input and  $\mathbf{u}_\Delta$  is the auxiliary vector reflecting the coupling between the quadrotors' translation and rotation. Therefore, from (34), the virtual control inputs can be designed as follows:

$$\mathbf{u} = -K_p e_\xi - K_d \dot{e}_\xi - \dot{\theta}_s^2 k_s \dot{e}_\xi + \mathbf{G}_t + \hat{\boldsymbol{\Phi}} \quad (35)$$

where  $K_d = \text{diag}([k_{dx1}, k_{dy1}, k_{dz1}, k_{dx2}, k_{dy2}, k_{dz2}]) \in \mathbb{R}^6$  is the positive control gain matrix and  $k_s$  is the positive control gain constant.

*Remark 1:* For the aerial collaborative transportation system, the lateral forces generated by the cargo along with the cables will continuously pull the aircraft closer to each other. The cable tensions vary with the system configuration and are related to the positions of the quadrotors. Nevertheless, traditional methods only consider the static compensation term in the specific desired state, and the change in lateral forces cannot be compensated in real-time. To this end,  $\mathbf{G}_t$  is constructed in (35) to represent the dynamic compensation term for lateral forces.

#### IV. STABILITY AND CONVERGENCE ANALYSIS

The stability proof of the closed-loop system is presented in this section.

*Theorem 1:* The proposed control input  $\mathbf{u}$  in (35) guarantees accurate quadrotors' positioning and cargo swing elimination in the sense that

$$\lim_{t \rightarrow \infty} [e_{\xi 1}^\top, e_{\xi 2}^\top, \dot{e}_{\xi 1}^\top, \dot{e}_{\xi 2}^\top, \dot{\theta}_s, \dot{\theta}_s]^\top = [0_{3 \times 1}^\top, 0_{3 \times 1}^\top, 0_{3 \times 1}^\top, 0_{3 \times 1}^\top, 0, 0]^\top.$$

*Proof:* The hierarchical control theory can be adopted by viewing the actual attitude and the expected attitude as identical [40], [41], [42], which means that the coupling term  $\mathbf{u}_\Delta$  can be temporarily neglected, i.e.,  $\mathbf{u}_\Delta = \mathbf{0}$ . Selecting (31) as the Lyapunov function candidate. Substituting the control inputs

(35) into (34), one can conclude as follows:

$$\begin{aligned} \dot{V} &= \dot{e}_\xi^\top \left( -K_p e_\xi - K_d \dot{e}_\xi - \dot{\theta}_s^2 k_s \dot{e}_\xi + G_t \right. \\ &\quad \left. + \hat{\Phi} - G_t + K_p e_\xi - \hat{\Phi} \right) - \dot{\theta}_s^2 \rho_7^\top D_c \rho_7 \\ &= -\dot{e}_\xi^\top \left( K_d + \dot{\theta}_s^2 k_s \right) \dot{e}_\xi - \dot{\theta}_s^2 \rho_7^\top D_c \rho_7 \leq 0 \end{aligned} \quad (36)$$

which indicates that  $V$  is nonincreasing, i.e.,

$$V(t) \leq V(0) \ll +\infty. \quad (37)$$

Combining the results in (18) and (31), the position errors and spatial swing angle are bounded, which can be presented as follows:

$$e_{\xi 1}, e_{\xi 2}, \dot{e}_{\xi 1}, \dot{e}_{\xi 2}, \theta_s, \dot{\theta}_s, \tilde{\omega}_{x1}, \tilde{\omega}_{y1}, \tilde{\omega}_{z1}, \tilde{\omega}_{x2}, \tilde{\omega}_{y2}, \tilde{\omega}_{z2} \in \mathcal{L}_\infty. \quad (38)$$

Therewith, define  $\Phi$  as follows:

$$\Phi = \left\{ (e_{\xi 1}, e_{\xi 2}, \dot{e}_{\xi 1}, \dot{e}_{\xi 2}, \theta_s, \dot{\theta}_s) \mid \dot{V}(t) = 0 \right\}. \quad (39)$$

Let  $\Gamma$  be the largest invariant set in  $\Phi$ , based on (36), the following conclusions can be achieved:

$$\begin{aligned} \dot{e}_{x1} = \dot{e}_{y1} = \dot{e}_{z1} = \dot{e}_{x2} = \dot{e}_{y2} = \dot{e}_{z2} &= 0 \Rightarrow \\ e_{x1} = \beta_{x1}, e_{y1} = \beta_{y1}, e_{z1} = \beta_{z1}, e_{x2} = \beta_{x2}, e_{y2} = \beta_{y2}, \\ e_{z2} = \beta_{z2}, \ddot{e}_{x1} = \ddot{e}_{y1} = \ddot{e}_{z1} = \ddot{e}_{x2} = \ddot{e}_{y2} = \ddot{e}_{z2} &= 0 \end{aligned} \quad (40)$$

where  $\beta_{x1}, \beta_{y1}, \beta_{z1}, \beta_{x2}, \beta_{y2}$ , and  $\beta_{z2}$  are undetermined constants. By substituting the above conclusions into the dynamics of the system (9), according to (16), it can be obtained that:

$$\frac{m_o g L d_p \sin \theta_s}{d} = 0. \quad (41)$$

In practical application, the horizontal distance  $d_p = \sqrt{(x_2 - x_1)^2 + (y_2 - y_1)^2}$  and spatial distance  $d = \|\xi_2 - \xi_1\|$  of quadrotors are both positive values. As the cargo is always underneath the two quadrotors, i.e.,  $L = \sqrt{(l_1)^2 - (d_m d)^2} > 0$ . Therefore, based on (41), the following conclusion can be obtained:

$$\sin \theta_s = 0 \Rightarrow \theta_s = 0 \Rightarrow \dot{\theta}_s = 0. \quad (42)$$

In the invariant set  $\Gamma$ , based on (40), the control inputs (35) can be expressed as follows:

$$\begin{aligned} u_{x1} &= -k_{px1} \beta_{x1} + m_o g \frac{\Delta x \Delta z (2d_m - 1)}{d^2} + G_{o1} \\ u_{y1} &= -k_{py1} \beta_{y1} + m_o g \frac{\Delta y \Delta z (2d_m - 1)}{d^2} + G_{o2} \\ u_{z1} &= -k_{pz1} \beta_{z1} + m_o g \left( 1 - \frac{\Delta z^2 (1 - 2d_m)}{d^2} - d_m \right) \\ &\quad + m_1 g + G_{o3} \\ u_{x2} &= -k_{px2} \beta_{x2} - m_o g \frac{\Delta x \Delta z (2d_m - 1)}{d^2} + G_{o4} \\ u_{y2} &= -k_{py2} \beta_{y2} - m_o g \frac{\Delta y \Delta z (2d_m - 1)}{d^2} + G_{o5} \\ u_{z2} &= -k_{pz2} \beta_{z2} + m_o g \left( \frac{\Delta z^2 (1 - 2d_m)}{d^2} + d_m \right) \end{aligned}$$

$$+ m_2 g + G_{o6}$$

where  $u_{x1}, u_{y1}, u_{z1}, u_{x2}, u_{y2}$ , and  $u_{z2}$  denote the components of  $\mathbf{u}$ . Inserting the control components into the dynamics of system (9) yields as follows:

$$\begin{aligned} \Delta x m_o g (1 - \cos \theta_s) \left[ -\frac{d_p L}{d^3} + \frac{L}{d_p d} + \frac{d_p d_m (d_m - 1)}{d L} \right] \\ = -k_{px1} \beta_{x1} \end{aligned} \quad (43)$$

$$\begin{aligned} \Delta y m_o g (1 - \cos \theta_s) \left[ -\frac{d_p L}{d^3} + \frac{L}{d_p d} + \frac{d_p d_m (d_m - 1)}{d L} \right] \\ = -k_{py1} \beta_{y1} \end{aligned} \quad (44)$$

$$\Delta z m_o g (1 - \cos \theta_s) \left[ -\frac{d_p L}{d^3} + \frac{d_p d_m (d_m - 1)}{d L} \right] = -k_{pz1} \beta_{z1} \quad (45)$$

$$\begin{aligned} \Delta x m_o g (1 - \cos \theta_s) \left[ \frac{d_p L}{d^3} - \frac{L}{d_p d} - \frac{d_p d_m (d_m - 1)}{d L} \right] \\ = -k_{px2} \beta_{x2} \end{aligned} \quad (46)$$

$$\begin{aligned} \Delta y m_o g (1 - \cos \theta_s) \left[ \frac{d_p L}{d^3} - \frac{L}{d_p d} - \frac{d_p d_m (d_m - 1)}{d L} \right] \\ = -k_{py2} \beta_{y2} \end{aligned} \quad (47)$$

$$\Delta z m_o g (1 - \cos \theta_s) \left[ \frac{d_p L}{d^3} - \frac{d_p d_m (d_m - 1)}{d L} \right] = -k_{pz2} \beta_{z2}. \quad (48)$$

According to (42) and (43)–(48), the following conclusions can be obtained:

$$\beta_{x1}, \beta_{y1}, \beta_{z1}, \beta_{x2}, \beta_{y2}, \beta_{z2} = 0 \quad (49)$$

which indicates that

$$e_{x1} = 0, e_{y1} = 0, e_{z1} = 0, e_{x2} = 0, e_{y2} = 0, e_{z2} = 0. \quad (50)$$

Hereto, from (40), (42), and (50), it is known that the largest invariant set  $\Gamma$  only contains the equilibrium point, i.e.,

$$\left[ e_{\xi 1}^\top, e_{\xi 2}^\top, \dot{e}_{\xi 1}^\top, \dot{e}_{\xi 2}^\top, \theta_s, \dot{\theta}_s \right]^\top = \left[ \mathbf{0}_{3 \times 1}^\top, \mathbf{0}_{3 \times 1}^\top, \mathbf{0}_{3 \times 1}^\top, \mathbf{0}_{3 \times 1}^\top, 0, 0 \right]^\top.$$

According to LaSalle's invariance principle [43], one can obtain that the equilibrium point of the system is asymptotically stable, and the proof of Theorem 1 is completed. ■

## V. EXPERIMENT AND RESULTS

In this section, experimental tests are conducted to verify the effectiveness of the proposed control method.

### A. General Experimental Platform Based on Onboard Sensors

As shown in Fig. 2, the general experimental platform is mainly composed of the visual-inertial navigation positioning system, the spatial swing angle measurement device, and the aerial transportation system with dual quadrotors.

1) *Location Technique Based on Onboard Visual Inertial Navigation*: Visual-inertial odometry (VIO) is a computer vision technique for estimating the 3-D pose of robots or objects, which is usually used for positioning and navigation in the case of



Fig. 2. General experimental platform.

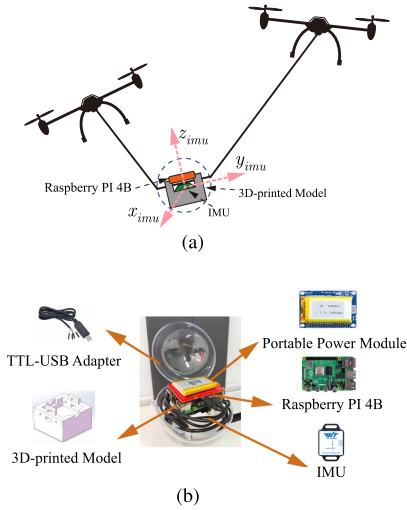


Fig. 3. Spatial swing angle measurement device. (a) Installation in-drone. (b) Hardware configuration.

missing or unreliable GPS signals (such as flying indoors or under bridges) by combining the images of the camera with the results of IMU. In this experiment, the binocular camera Intel RealSense T265 is utilized to acquire the location data of the quadrotors, and the robot operating system (ROS) topics containing poses of quadrotors are sent to the ground station through the on-board computers Jetson Xavier NX.

**2) Spatial Swing Angle Measurement Device:** The inertial measurement unit (IMU) is placed on the cargo, which can feed back the cargo dynamics in real time. The cargo spatial swing angle measurement device is mainly composed of the IMU, the mini onboard computer Raspberry PI 4B with the portable power module, and the 3-D-printed model, which is presented in Fig. 3. The main role of the 3-D-printed model is to keep the IMU fixed on the cargo. Through the careful design of the IMU installation method, the rotation angle along the  $y_{imu}$ -axis in the IMU body coordinate is the spatial swing angle. The angle and angular velocity data obtained by the IMU are transferred to the Raspberry PI via the TTL-USB adapter, while relevant ROS topics are published by the Raspberry PI, so as to realize the real-time feedback of spatial swing angle data.

**3) Aerial Transportation System With Dual Quadrotors:** As mentioned above, the data of quadrotor positions are obtained by onboard VIO, while the data of spatial swing angle is measured by the IMU. All feedback data are sent to the ground station

based on the local area network with the form of ROS messages. The ground station transmits the control inputs to the onboard computers via WIFI with 5G band. The frequency of the data transmitting among them is 100 Hz. The onboard computers are connected to the flight controllers Pixhawk by mavros based communication protocol.

## B. Experimental Results and Analysis

In this section, several groups of experiments are implemented in indoor and outdoor environments to validate the effectiveness and adaptability of the proposed control scheme. The experimental video is available online.<sup>1</sup>

**1) Indoor Experiment:** First, the verification work is carried out in the indoor environment. The physical parameters of the aerial transportation system are chosen as follows:  $m_1 = 1.675$  kg,  $m_2 = 1.675$  kg,  $m_o = 0.43$  kg,  $l_1 = 1.68$  m,  $l_2 = 1.71$  m, and  $g = 9.8$  m/s<sup>2</sup>. The initial positions and desired positions of quadrotors are set as  $\xi_1(0) = [-1.0, -0.3, 1.54]^T$  m,  $\xi_2(0) = [-0.6, 1.0, 1.54]^T$  m,  $\xi_{1d} = [1.0, -0.7, 1.8]^T$  m, and  $\xi_{2d} = [1.4, 0.6, 1.8]^T$  m. The controller gains are set as  $k_{px1} = 3.7$ ,  $k_{py1} = 3.8$ ,  $k_{pz1} = 8.0$ ,  $k_{px2} = 3.7$ ,  $k_{py2} = 3.8$ ,  $k_{pz2} = 8.0$ ,  $k_{dx1} = 5.5$ ,  $k_{dy1} = 6.0$ ,  $k_{dz1} = 10.5$ ,  $k_{dx2} = 5.5$ ,  $k_{dy2} = 6.0$ ,  $k_{dz2} = 10.5$ ,  $k_s = 1.2$ ,  $\Gamma_{x1} = \text{diag}([1.6, 1.6])$ ,  $\Gamma_{y1} = \text{diag}([1.4, 1.4])$ ,  $\Gamma_{z1} = \text{diag}([0.9, 0.9])$ ,  $\Gamma_{x2} = \text{diag}([1.6, 1.6])$ ,  $\Gamma_{y2} = \text{diag}([1.4, 1.4])$ , and  $\Gamma_{z2} = \text{diag}([0.9, 0.9])$ . The PID-based controller is selected as the comparison method, whose control gains are selected as:  $K_{pPID} = \text{diag}([3.7, 3.8, 8.0, 3.7, 3.8, 8.0])$ ,  $K_{iPID} = \text{diag}([1.0, 1.0, 4.0, 1.0, 1.0, 4.0])$ , and  $K_{dPID} = \text{diag}([5.5, 6.0, 10.5, 5.5, 6.0, 10.5])$ . The curves of the indoor experimental results are presented in Fig. 4, which includes the space swing angle, the estimates of air drag coefficients, and the positions as well as the control inputs of both quadrotors. From Fig. 4(a), one can find that both methods can drive the quadrotors to the desired positions. The explicit quantified data are recorded in Table I,  $|\theta_s|_{\max}$  represents the maximum absolute value of the cargo swing amplitude,  $|\bar{\theta}_s|$  denotes the mean absolute value of the swing angles.  $t_s$  represents the anti-swing time, it is the time when the absolute value of the swing angle remains consistently less than  $5^\circ$ .  $\bar{e}_{\xi_1}$  and  $\bar{e}_{\xi_2}$  are the mean tracking errors of the two quadrotors, which are the mean absolute values of the quadrotors' tracking errors from 6 to 17 s. It can be seen from the table that with similar quadrotors' position tracking errors, the proposed method has a faster anti-swing time and smaller maximum swing angle. The maximum absolute value of cargo swing amplitude reveals that the PID controller's maximum cargo swing amplitude is nearly twice that of the proposed method. As observed from the results of swing amplitude and mean value of the space swing angle, the proposed method has a better anti-swing performance compared with the PID controller.

**2) Outdoor Experiment:** In order to verify the performance of the proposed control method in practical application, a group of outdoor experiments are carried out based on the self-built experimental platform, and the physical parameters are same as the indoor experiments.

The initial positions and desired positions of quadrotors are set as  $\xi_1(0) = [0.0, -0.8, 1.7]^T$  m,  $\xi_2(0) = [0.0, 0.7, 1.7]^T$  m,  $\xi_{1d} = [1.75, -1.5, 2.0]^T$  m, and  $\xi_{2d} = [1.75, 0.0, 2.0]^T$  m. The

<sup>1</sup>[Online]. Available at: <https://youtu.be/5kxyVRB9G50>



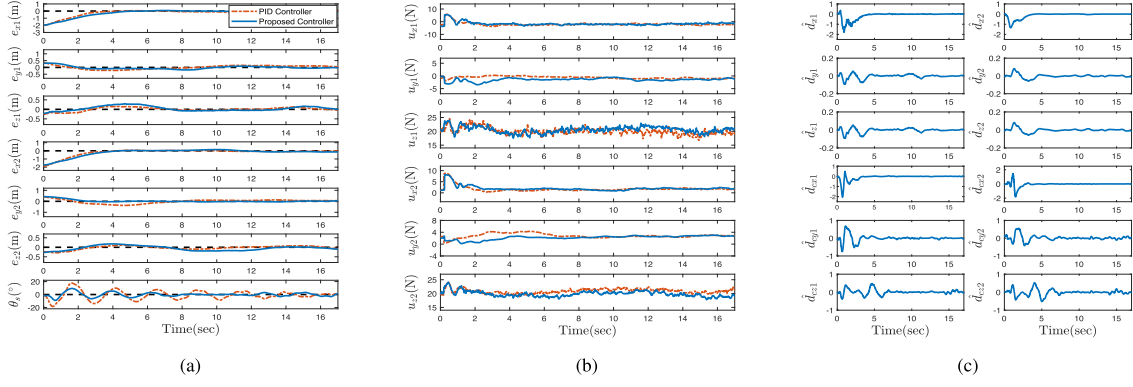


Fig. 4. Results for *Indoor Experiment*. (a) Quadrotors position error and cargo swing angle. (b) Control inputs. (c) Estimation of air drag coefficients.

TABLE I  
QUANTITATIVE DATA

		$ \theta_s _{\max} (^{\circ})$	$\bar{ \theta_s } (^{\circ})$	$t_s (s)$	$\bar{e}_{\xi 1} (m)$	$\bar{e}_{\xi 2} (m)$
Indoor Exp.	Pro.	<b>9.38</b>	<b>2.27</b>	<b>4.10</b>	$[0.08, 0.08, 0.07]^T$	$[0.09, 0.02, 0.09]^T$
	PID	18.42	5.28	12.93	$[0.10, 0.10, 0.04]^T$	$[0.05, 0.09, 0.05]^T$
Outer Exp.	Pro.	<b>9.49</b>	<b>2.18</b>	<b>7.92</b>	$[0.06, 0.19, 0.03]^T$	$[0.10, 0.13, 0.03]^T$
	PID	17.55	4.88	12.33	$[0.08, 0.12, 0.04]^T$	$[0.06, 0.07, 0.06]^T$

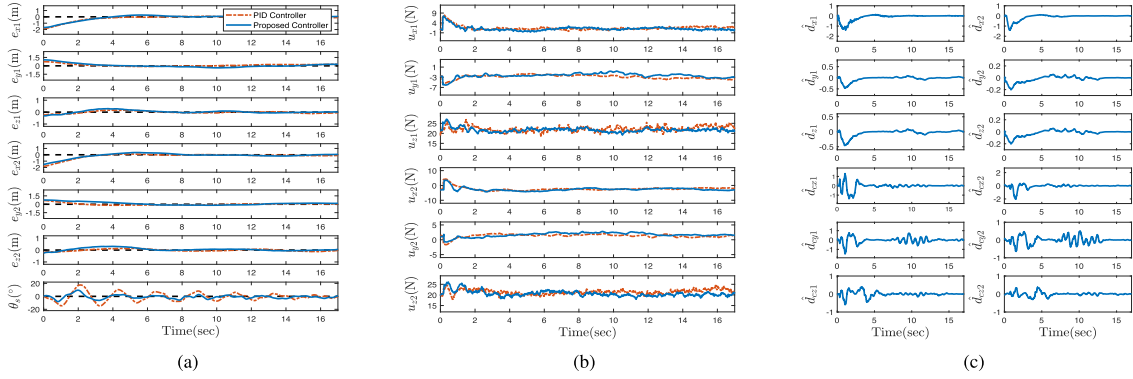


Fig. 5. Results for *Outdoor Experiment*. (a) Quadrotors position error and cargo swing angle. (b) Control inputs. (c) Estimation of air drag coefficients.

controller gains are set as  $k_{px1} = 3.7$ ,  $k_{py1} = 3.8$ ,  $k_{pz1} = 8.0$ ,  $k_{px2} = 3.7$ ,  $k_{py2} = 3.8$ ,  $k_{pz2} = 8.0$ ,  $k_{dx1} = 5.5$ ,  $k_{dy1} = 6.0$ ,  $k_{dz1} = 10.5$ ,  $k_{dx2} = 5.5$ ,  $k_{dy2} = 6.0$ ,  $k_{dz2} = 10.5$ , and  $k_s = 0.9$ . The adaptive update gains are selected as  $\Gamma_{x1} = \text{diag}([1.6, 1.6])$ ,  $\Gamma_{y1} = \text{diag}([1.6, 1.6])$ ,  $\Gamma_{z1} = \text{diag}([1.5, 1.5])$ ,  $\Gamma_{x2} = \text{diag}([1.6, 1.6])$ ,  $\Gamma_{y2} = \text{diag}([1.6, 1.6])$ , and  $\Gamma_{z2} = \text{diag}([1.5, 1.5])$ . The PID controller is chosen as the comparison method, and the control gains are selected the same as the indoor experiment. The curves of the outdoor experimental results are presented in Fig. 5, which includes the space swing angle, the quadrotors' position errors, the control inputs of quadrotors as well as the estimates of air drag coefficients. The results of Fig. 5(a) indicate that both methods can drive the quadrotors to the desired positions. Moreover, it can be seen that the spatial swing angle converges within 12.33 s by the PID method, while the spatial swing angle is suppressed within only 7.92 s by the proposed method. Compared with the PID method, the proposed method can effectively suppress the cargo swing due to the spatial swing angle damping term in (35), and the estimation

and compensation of the air resistance coefficients during flight. It is worth noting that the outdoor environment is more complex and exists various airflow disturbances, the accurate estimation of the air resistance of the system is beneficial to improve the control performance of the system.

## VI. CONCLUSION

This article focuses on the aerial collaborative transportation with dual quadrotors and introduces the spatial swing angle to describe the dynamics of the cargo. Compared with the description of cargo swing dynamics with four angles in the previous work [35], the spatial swing angle introduced in this article can intuitively reflect the swing dynamics of the cargo. In addition, considering the measurement method of cargo swing in practical applications, the information of the spatial swing angle is more convenient to obtain. Specifically, the dynamic model of the system based on the spatial swing angle is established by using Lagrange's equation. Subsequently, a nonlinear adaptive



controller is designed on the basis of energy analysis, which introduces a dynamic compensation term to compensate for the lateral forces along the cables and a spatial swing angle-related term to improve cargo swing damping. Meanwhile, considering the influence of unknown air resistance on quadrotors and cargo during transportation, an adaptive term is applied. Lyapunov techniques and LaSalle's invariance principle are used to prove the stability of the closed-loop system. Finally, a self-built experimental platform applicable for both indoor and outdoor environments is designed, and the effectiveness of the proposed method is verified. In the future, trajectory tracking control schemes with theoretical analysis will be taken into account for collaborative aerial transportation systems.

## REFERENCES

- [1] Y. Yuan and H. Duan, "Adaptive learning control for a quadrotor unmanned aerial vehicle landing on a moving ship," *IEEE Trans. Ind. Informat.*, vol. 20, no. 1, pp. 534–545, Jan. 2024.
- [2] Y. Yang, S. Gorbachev, B. Zhao, Q. Liu, Z. Shu, and D. Yue, "Predictor-based neural attitude control of a quadrotor with disturbances," *IEEE Trans. Ind. Informat.*, vol. 20, no. 1, pp. 169–178, Jan. 2024.
- [3] S. Sun, A. Romero, P. Foehn, E. Kaufmann, and D. Scaramuzza, "A comparative study of nonlinear MPC and differential-flatness-based control for quadrotor agile flight," *IEEE Trans. Robot.*, vol. 38, no. 6, pp. 3357–3373, Dec. 2022.
- [4] Y. Zhang, L. Ma, C. Yang, L. Zhou, G. Wang, and W. Dai, "Formation control for multiple quadrotors under DoS attacks via singular perturbation," *IEEE Trans. Aerosp. Electron. Syst.*, vol. 59, no. 4, pp. 4753–4762, Aug. 2023.
- [5] J. Guo, J. Qi, M. Wang, C. Wu, and G. Yang, "Collision-free distributed control for multiple quadrotors in cluttered environments with static and dynamic obstacles," *IEEE Robot. Autom. Lett.*, vol. 8, no. 3, pp. 1501–1508, Mar. 2023.
- [6] S. Yang, B. Xian, J. Cai, and G. Wang, "Finite-time convergence control for a quadrotor unmanned aerial vehicle with a slung load," *IEEE Trans. Ind. Informat.*, vol. 20, no. 1, pp. 605–614, Jan. 2024.
- [7] J. Zeng, P. Kotaru, and K. Sreenath, "Geometric control and differential flatness of a quadrotor UAV with load suspended from a pulley," in *Proc. 2019 Amer. Control Conf.*, 2019, pp. 2420–2427.
- [8] Y. Gu, K. Guo, C. Zhao, X. Yu, and L. Guo, "Fast reactive mechanism for desired trajectory attacks on unmanned aerial vehicles," *IEEE Trans. Ind. Informat.*, vol. 19, no. 8, pp. 8976–8984, Aug. 2023.
- [9] J. Thomas, G. Loianio, K. Sreenath, and V. Kumar, "Toward image based visual servoing for aerial grasping and perching," in *Proc. 2014 IEEE Int. Conf. Robot. Automat.*, 2014, pp. 2113–2118.
- [10] D. Mellinger, Q. Lindsey, M. Shomin, and V. Kumar, "Design, modeling, estimation and control for aerial grasping and manipulation," in *Proc. 2011 IEEE/RSJ Int. Conf. Intell. Robots Syst.*, 2011, pp. 2668–2673.
- [11] P. O. Pereira, R. Zanella, and D. V. Dimarogonas, "Decoupled design of controllers for aerial manipulation with quadrotors," in *Proc. 2016 IEEE/RSJ Int. Conf. Intell. Robots Syst.*, 2016, pp. 4849–4855.
- [12] Y. Chen, J. Liang, Y. Wu, Z. Miao, H. Zhang, and Y. Wang, "Adaptive sliding-mode disturbance observer-based finite-time control for unmanned aerial manipulator with prescribed performance," *IEEE Trans. Cybern.*, vol. 53, no. 5, pp. 3263–3276, May 2023.
- [13] H. Lee and H. J. Kim, "Constraint-based cooperative control of multiple aerial manipulators for handling an unknown payload," *IEEE Trans. Ind. Informat.*, vol. 13, no. 6, pp. 2780–2790, Dec. 2017.
- [14] M. Jafarinasab, S. Sirouspour, and E. Dyer, "Model-based motion control of a robotic manipulator with a flying multirotor base," *IEEE/ASME Trans. Mechatron.*, vol. 24, no. 5, pp. 2328–2340, Oct. 2019.
- [15] J. Potter, W. Singhose, and M. Costelloy, "Reducing swing of model helicopter sling load using input shaping," in *Proc. 2011 9th IEEE Int. Conf. Control Automat.*, 2011, pp. 348–353.
- [16] I. Palunko, R. Fierro, and P. Cruz, "Trajectory generation for swing-free maneuvers of a quadrotor with suspended payload: A dynamic programming approach," in *Proc. 2012 IEEE Int. Conf. Robot. Automat.*, 2012, pp. 2691–2697.
- [17] I. Palunko, P. Cruz, and R. Fierro, "Agile load transportation: Safe and efficient load manipulation with aerial robots," *IEEE Robot. Automat. Mag.*, vol. 19, no. 3, pp. 69–79, Sep. 2012.
- [18] B. S. Rego, D. M. Raimondo, and G. V. Raffo, "Path tracking control with state estimation based on constrained zonotopes for aerial load transportation," in *Proc. 2018 IEEE Conf. Decis. Control*, 2018, pp. 1979–1984.
- [19] Z. Lv, Y. Wu, X.-M. Sun, and Q.-G. Wang, "Fixed-time control for a quadrotor with a cable-suspended load," *IEEE Trans. Intell. Transp. Syst.*, vol. 23, no. 11, pp. 21932–21943, Nov. 2022.
- [20] S. Yang and B. Xian, "Energy-based nonlinear adaptive control design for the quadrotor UAV system with a suspended payload," *IEEE Trans. Ind. Electron.*, vol. 67, no. 3, pp. 2054–2064, Mar. 2020.
- [21] H. Yu, X. Liang, J. Han, and Y. Fang, "Adaptive trajectory tracking control for the quadrotor aerial transportation system landing a payload onto the mobile platform," *IEEE Trans. Ind. Informat.*, vol. 20, no. 1, pp. 23–37, Jan. 2024.
- [22] I. Palunko, A. Faust, P. Cruz, L. Tapia, and R. Fierro, "A reinforcement learning approach towards autonomous suspended load manipulation using aerial robots," in *Proc. 2013 IEEE Int. Conf. Robot. Automat.*, 2013, pp. 4896–4901.
- [23] V. P. Tran, F. Santoso, M. A. Garrat, and S. G. Anavatti, "Neural network-based self-learning of an adaptive strictly negative imaginary tracking controller for a quadrotor transporting a cable-suspended payload with minimum swing," *IEEE Trans. Ind. Electron.*, vol. 68, no. 10, pp. 10 258–10 268, Oct. 2021.
- [24] M. Gassner, T. Cieslewski, and D. Scaramuzza, "Dynamic collaboration without communication: Vision-based cable-suspended load transport with two quadrotors," in *Proc. 2017 IEEE Int. Conf. Robot. Automat.*, 2017, pp. 5196–5202.
- [25] T. Chen and J. Shan, "Cooperative transportation of cable-suspended slender payload using two quadrotors," in *Proc. 2019 IEEE Int. Conf. Unmanned Syst.*, 2019, pp. 432–437.
- [26] A. Tagliabue, M. Kamel, S. Verling, R. Siegwart, and J. Nieto, "Collaborative transportation using MAVs via passive force control," in *Proc. 2017 IEEE Int. Conf. Robot. Automat.*, 2017, pp. 5766–5773.
- [27] T. Baccelar, J. Madeiras, R. Melicio, C. Cardeira, and P. Oliveira, "On-board implementation and experimental validation of collaborative transportation of loads with multiple UAVs," *Aerosp. Sci. Technol.*, vol. 107, 2020, Art. no. 106284.
- [28] D. K. D. Villa, A. S. Brandão, R. Carelli, and M. S.-Filho, "Cooperative load transportation with two quadrotors using adaptive control," *IEEE Access*, vol. 9, pp. 129 148–129 160, 2021.
- [29] F. Rossomando et al., "Aerial load transportation with multiple quadrotors based on a kinematic controller and a neural smc dynamic compensation," *J. Intell. Robot. Syst.*, vol. 100, pp. 519–530, 2020.
- [30] M. D. Takahashi, M. S. Whalley, M. G. Berrios, and G. J. Schulein, "Flight validation of a system for autonomous rotorcraft multilift," *J. Amer. Helicopter Soc.*, vol. 64, no. 3, pp. 1–13, 2019.
- [31] J. Gimenez, D. C. Gandolfo, L. R. Salinas, C. Rosales, and R. Carelli, "Multi-objective control for cooperative payload transport with rotorcraft UAVs," *ISA Trans.*, vol. 80, pp. 491–502, 2018.
- [32] T. Lee, "Geometric control of quadrotor UAVs transporting a cable-suspended rigid body," *IEEE Trans. Control Syst. Technol.*, vol. 26, no. 1, pp. 255–264, Jan. 2018.
- [33] X. Jin and Z. Hu, "Constrained load transportation by a team of quadrotors," in *Proc. 2022 IEEE 61st Conf. Decis. Control*, 2022, pp. 6580–6585.
- [34] Y. Chai, X. Liang, Z. Yang, and J. Han, "Energy-based nonlinear adaptive control for collaborative transportation systems," *Aerosp. Sci. Technol.*, vol. 126, 2022, Art. no. 107510.
- [35] X. Liang, Z. Zhang, H. Yu, Y. Wang, Y. Fang, and J. Han, "Antiswing control for aerial transportation of the suspended cargo by dual quadrotor UAVs," *IEEE/ASME Trans. Mechatron.*, vol. 27, no. 6, pp. 5159–5172, Dec. 2022.
- [36] K. Wahba and W. Hönig, "Efficient optimization-based cable force allocation for geometric control of a multirotor team transporting a payload," *IEEE Robot. Autom. Lett.*, vol. 9, no. 4, pp. 3688–3695, Apr. 2024.
- [37] G. Yu, J. Reis, D. Cabecinhas, R. Cunha, and C. Silvestre, "Reduced-complexity active disturbance rejection controller for quadrotor-slung-load transportation," *IEEE Trans. Syst., Man, Cybern. Syst.*, vol. 53, no. 8, pp. 5248–5259, Aug. 2023.
- [38] A. Akhtar, S. Saleem, and J. Shan, "Path following of a quadrotor with a cable-suspended payload," *IEEE Trans. Ind. Electron.*, vol. 70, no. 2, pp. 1646–1654, Feb. 2023.

- [39] L. Sun et al., "A novel tension-based controller design for the quadrotor-load system," *Control Eng. Pract.*, vol. 112, 2021, Art. no. 104818.
- [40] F. Kendoul, "Nonlinear hierarchical flight controller for unmanned rotorcraft: Design, stability, and experiments," *J. Guid., Control, Dyn.*, vol. 32, no. 6, pp. 1954–1958, 2009.
- [41] B. Zhao, B. Xian, Y. Zhang, and X. Zhang, "Nonlinear robust adaptive tracking control of a quadrotor UAV via immersion and invariance methodology," *IEEE Trans. Ind. Electron.*, vol. 62, no. 5, pp. 2891–2902, May 2015.
- [42] B. Zhao, B. Xian, Y. Zhang, and X. Zhang, "Nonlinear robust sliding mode control of a quadrotor unmanned aerial vehicle based on immersion and invariance method," *Int. J. Robust Nonlinear Control*, vol. 25, no. 18, pp. 3714–3731, 2015.
- [43] H. K. Khalil, *Nonlinear Systems*. Upper Saddle River, NJ, USA: Prentice-Hall, 2002.



**Zhuang Zhang** received the B.S. degree in intelligence science and technology from the Hebei University of Technology, Tianjin, China, in 2020, and the M.S. degree in control science and engineering from Nankai University, Tianjin, in 2023.

His research interests include nonlinear control of multi-micro-unmanned aerial vehicles.



**Hai Yu** (Student Member, IEEE) received the B.S. degree in automation from Jilin University, Changchun, China, in 2020. He is currently working toward the Ph.D. degree in control science and engineering with the Institute of Robotics and Automatic Information System, Nankai University, Tianjin, China.

His research interests include motion planning and nonlinear control of unmanned aerial vehicles.



**Huiying Ye** received the B.S. degree in automation in 2023 from Nankai University, Tianjin, China, where she is currently working toward the M.S. degree in control science and engineering with the Institute of Robotics and Automatic Information System.

Her research interest focuses on nonlinear control of unmanned aerial vehicles.



**Jianda Han** (Member, IEEE) received the Ph.D. degree in mechatronic engineering from Harbin Institute of Technology, Harbin, China, in 1998.

From 1998 to 2003, he was a Visiting Scientist with the City University of Hong Kong, Hong Kong; Michigan State University, East Lansing, MI, USA, and Cornell University, Ithaca, NY, USA. He is currently a Professor with the Institute of Robotics and Automatic Information System, Nankai University, Tianjin, China. His research interests include nonlinear estimation

and control, robotics, and mechatronics systems.



**Yongchun Fang** (Senior Member, IEEE) received the B.S. and M.S. degrees in control theory and applications from Zhejiang University, Hangzhou, China, in 1996 and 1999, respectively, and the Ph.D. degree in electrical engineering from Clemson University, Clemson, SC, USA, in 2002.

From 2002 to 2003, he was a Postdoctoral Fellow with the Sibley School of Mechanical and Aerospace Engineering, Cornell University, Ithaca, NY, USA. He is currently a Professor with

the Institute of Robotics and Automatic Information System, Nankai University, Tianjin, China. His research interests include nonlinear control, visual servoing, control of underactuated systems, and atomic force microscopy (AFM)-based nanosystems.

Dr. Fang was the recipient of the National Science Fund for Distinguished Young Scholars of China. He was an Associate Editor of the *ASME Journal of Dynamic Systems, Measurement, and Control*.



**Xiao Liang** (Senior Member, IEEE) received the B.S. degree in intelligence science and technology from the Hebei University of Technology, Tianjin, China, in 2013, and the Ph.D. degree in control theory and control engineering from Nankai University, Tianjin, in 2018.

He is currently an Associate Professor with the Institute of Robotics and Automatic Information System, Nankai University. His research interests include motion planning and nonlinear control of unmanned aerial vehicle systems.